行政院國家科學委員會補助專題研究計畫成果報告

※※※※※※※※※※※※※※※※※※※※※※※※※※
※ 靜電式微機電振動-電能轉換器 ※
※※※※※※※※※※※※※※※※※※※※※※※※※※

計畫類別：□個別型計畫 ☑整合型計畫
計畫編號：NSC－96－2221－E－009－234
執行期間：96 年 8 月 1 日至 97 年 7 月 31 日

計畫主持人：邱一
共同主持人：
計畫參與人員：陳弘諳 張經富

執行單位：國立交通大學 電機與控制工程系

中 華 民 國 97 年 10 月 15 日

靜電式微機電振動-電能轉換器

"Design and Fabrication of a Micro Electrostatic Vibration-to-Electricity Energy Converter"

計畫編號：NSC96-2221-E-009-234

執行期間：96 年 8 月 1 日 至 97 年 7 月 31 日

主持人：邱一 交通大學電機與控制工程系副教授

一、中文摘要

微機電系統是以半導體產業中的平面製造觀念為基礎的一種整合技術。在無線感測網路等應用中，高度整合的可攜式元件都具有獨立電源的需求。拜先進的超大型積體電路技術所賜，這些微系統元件的電能需求已降至數十 μW 的程度。因此將環境中的能源轉換成電能來供給這些可攜式元件使用已經逐漸成為一個可行的方法

本年度計畫採用靜電式的微機電動能-電能轉換方式，針對測量到的 120 Hz, 2.25 m/s^2 的振動，在 300mV 輸入電源的條件下，於 1 cm^2 的晶片面積上及無外加質量塊的條件下，設計出輸出為 0.51 μW 的微型電源供應器。另外也搭配了機械式開關來提供準確的充放電能量轉換控制。此外，在元件製作方面，本年度將承接上一代的元件結構設計，設法改善原有的漏電現象，以得到更好的操作性能。製作上主要是利用 SOI 晶圓並搭配深蝕刻來製作完成。在功率量測方面，在無外加質量塊、5 MΩ 負載及 1730Hz 振動頻率條件下，量測到的交流輸出功率為 0.42μW，有承載外加質量的輸出功率及後續機械開關操作的量測目前正在進行中。

英文摘要

Micro-Electro-Mechanical System (MEMS) is a technology platform based on the planar fabrication process in the IC industry. In applications such as wireless sensor networks, highly integrated portable or remote devices need independent power supply. Due to recent advances in low power VLSI technology, the power consumption is reduced to a few tens of microwatts. Therefore, it becomes feasible to power the portable devices by scavenging the ambient energy.

The objective of this project is to develop an electrostatic MEMS vibration-to-electric energy converter with no external mass attachment on an area of 1 cm^2 and auxiliary power supply of 300mV. The targeted energy source is the 120 Hz, 2.25 m/s^2 vibration measured in household appliances. The device was designed to generate an output power of 0.51μW. Mechanical switches are integrated with the transducer unit to provide accurate energy conversion timing control. Furthermore, the previous design will be improved for better performance in this project. The device was fabricated in SOI wafers by deep silicon etching technology. Measurements of the energy converter were also conducted. Without the external mass, the measured AC output power was 0.42 μW with a load of 5 MΩ at 1730 Hz. AC output power measurement of the devices with external mass attached and subsequent mechanical switches measurement is in progress.

二、計畫的緣由與目的

Due to the advance of CMOS VLSI technology, the power consumption of electronic devices has been reduced considerably. The low power technology enables the development of such applications as wireless sensor networks [1] or personal health monitoring [2], where remote or independent power supply is critical for more compact or longer-life-time systems. In particular, energy scavenging from ambient natural sources, such as vibration [3], radioisotope [4] and ambient heat [5], is attracting many recent interests as the self-sustainable power sources. Among various approaches, electrostatic vibration-to-electricity conversion is chosen in this study due to its compatibility to IC processes and the ubiquity of the energy source in nature.

The output power of a vibration driven converter is related to the characteristics of the vibration source. A typical vibration found in many household appliances has a peak acceleration of about 2.25 m/s^2 at about 120 Hz. Therefore, this vibration is used as the energy source for the design of the optimal converter.

三、研究方法及成果

1 Design

The operation circuit of the converter is shown in Fig.1 [6]. The circuit composed of a 300mV auxiliary power supply V_{in}, a vibration-driven variable capacitor C_v and an output storage capacitor C_{stor} connected with the load R_L. C_v is charged by V_{in} through SW1 at its maximum C_{max}, and discharged to C_{stor} through SW2 at its minimum C_{min} when the terminal voltage is at its maximum V_{max}. To achieve high conversion efficiency, the charge-discharge cycles must be timed precisely with the change of the capacitance.

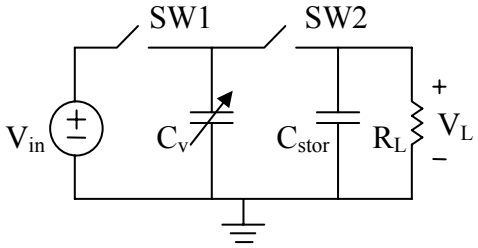

Fig. 1: Operation of the electrostatic energy converter

The variable capacitor C_v is formed by an in-plane gap-closing comb structure [7], as shown in Fig. 2(a). Silicon nitride dielectric coating (ε_r = 7) on finger sidewalls is applied to prevent shortage. The comb fingers are designed to have special "bumps" to maintain minimum air gap even under etching process inaccuracy, as shown in Fig. 2(b).

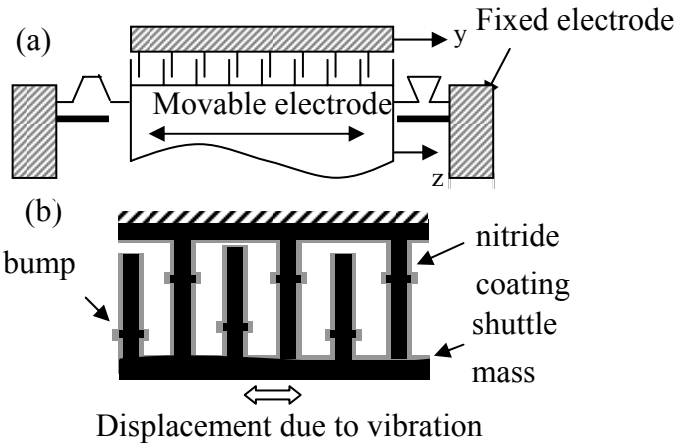

Fig. 2: (a) In-plane gap-closing comb structured variable capacitor schematic, (b) bumps on comb fingers

1.1 Static analysis

In the symmetric design with no external mass attached in the Fig. 3, the mass of the movable electrode and output power are

$$m = \rho h[2N_g W_f (L_f + d) + 8W_1 W_2 + (L_0 - 2W_1)W_0]$$

$$P_{out} = fC_{stor} V_{sat}^{\ 2}[\exp(\frac{1}{2fR_L C_{stor}}) - 1] \qquad (1)$$

where the W_1 is width of the electrode region in the x-direction, W_2 is the distance between two sets of electrodes in the y-direction, L_f is overlap length of fingers, d is initial gap between fingers, and f is vibration frequency. V_{sat} is output voltage which is related primarily to the variable maximum capacitor value C_{max}.

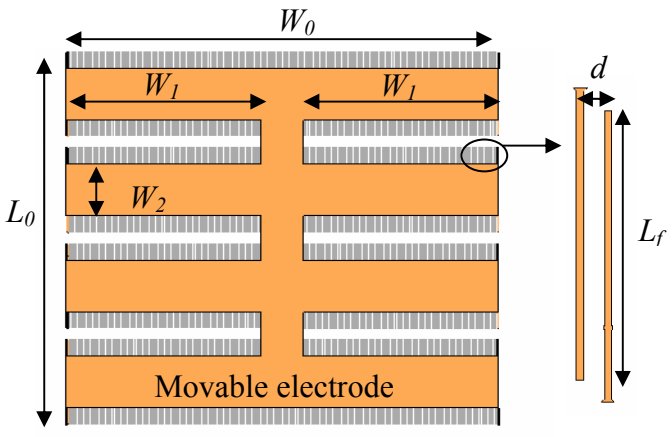

Fig. 3 Schematic of the energy converter

A number of free parameters must be considered to acquire the optimum output power in the schematic of Fig.3. The guideline of the optimization of parameters was presented in [8] and [9]. Thus, the output power is a function of initial finger gap distance d and overlap length of finger L_f, as shown in Fig. 4. Fig. 5 shows the maximum electrostatic spring constant caused by the constant charge Q on the variable capacitor C_v. It has great effects on the dynamic behaviour of the system since it will alter the mechanical spring constant of the system. According to the dynamic analysis, the spring constant can be presented as follow:

$$b_{e\_\max} \le \frac{4\pi^2 f^2 m(L_f, d)}{r_d} = \frac{k}{r_d}, \qquad (2)$$

where k is mechanical spring constant and r_d is the ratio between k and b_{e_max}. It is chiefly concerned with the maximum displacement between fingers. The detail will be discussed in the next section. Fig. 5 shows the maximum electrostatic spring constant limitation $b_{e\_max\_lim}$ and b_{e_max}. The electrostatic force and the electrostatic spring effect can be ignored if b_{e_max} is small than $b_{e\_max\_lim}$, shown as the available design region. According to the constraint for the electrostatic spring constant, the maximum output power is 0.51 μW with the initial gap of 37 μm and fingers overlap length of 535 μm in our device.

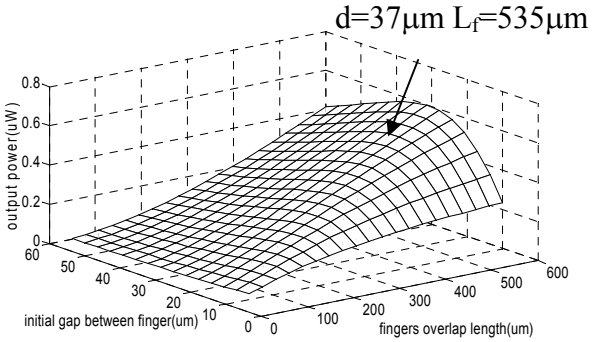

Fig. 4 Output power versus initial gap and fingers overlap length

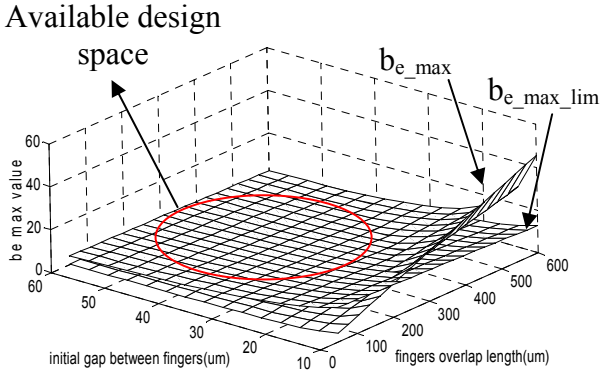

Fig.5 b_{e_max}, $b_{e\_max\_lim}$, and available design space under given constraints

1.2 Dynamic analysis

The dynamic analysis is used to decide the appropriate mechanical spring constant k and proof mass m in order to assure adequate displacement under the target vibration source during resonance. The equation can be described by

$$m\ddot{z}+b_e(z)+b_m(z,\dot{z})+kz=-m\ddot{y}, \quad (3)$$

Where z is the displacement of the shuttle mass with respect to the device frame, y is the displacement of the device frame caused by vibration, $b_m(z,\dot{z})$ is the mechanical damping force, and $b_e(z)$ is the electrostatic force acting on the MEMS structure.

The electrostatic force $b_e(z)$ acting on the structure is equivalent to a spring force with spring constant b_e, which alters its value during the charge-discharge cycles. The total equivalent spring constant of the system is $k' = k + b_{e\_max}$. In order to maintain steady resonance, the mechanical spring constant k should be larger than b_e. Fig. 6 shows the relation of the k/b_e ratio and the desired maximum displacement. The phenomenon also is discussed in [10]. The theoretical value is compared with simulation value from the Simulink model. It is also used to calculate the $b_{e\_max\_lim}$ graph in Fig 5..

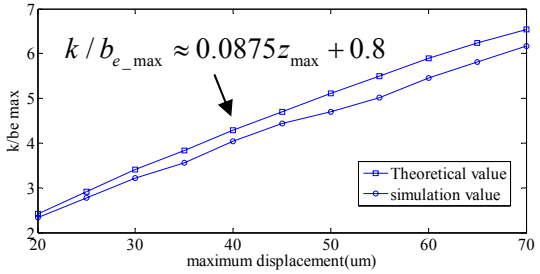

Fig. 6 k/b_{e_max} ratio versus desired maximum displacement

Timing control of the switches is also important for the energy conversion efficiency. When the variable capacitor moves to the middle position, SW2 should be turned on at the same time. If not, energy stored in the variable capacitor can not be fully transferred to C_{stor} and the output power is reduced. The simulated output power loss versus timing error is shown in Fig. 7.

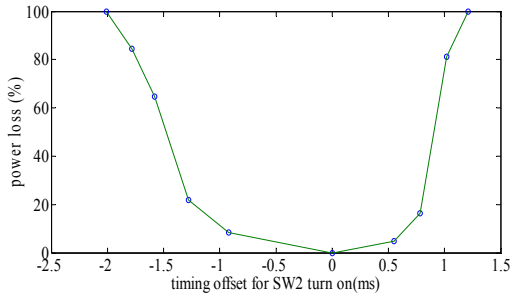

Fig.7 Output power loss versus timing error

2 Fabrication

The device is fabricated in a silicon-on-insulator (SOI) wafer with a 200-μm-thick low-resistance device layer. Device structure is defined by ICP (Inductively Coupled Plasma) etching. Nitride is deposited by LPCVD (Low Pressure Chemical Vapor Deposition). The back side handle layer is then removed by ICP etching to reduce parasitic capacitance. The structure is released by HF vapor. Sputtering of gold or aluminium with the shadow mask is done for metallic contact.

Compared to last year, the primary goal of this year is to reduce the overlap areas between the springs and mechanical switches to avoid the parasitic resistance. LPCVD was adapted due to good step coverage and insulation.

Fig. 8 shows the SEM micrograph of the

device after the ICP process. Fig. 9 shows the overview of whole device. The tungsten ball is attached to the center plate and positioned by the center hole on the device.

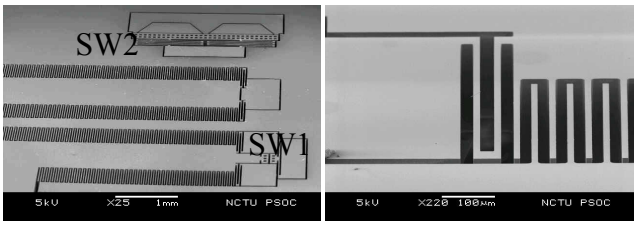

(a) (b)

Fig. 8: (a) Device overview, including comb fingers, spring, SW1 and SW2, (b) close-up view of fingers and spring,

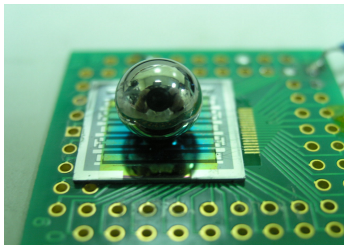

Fig. 9 Device with the external mass attached

3 Measurements

3.1 Mechanical measurement

The relative displacement of the device with a 4 gram tungsten ball was measured using the MMA (MEMS Motion Analyser). As shown in Fig. 10, the amplitude response has a resonant frequency around 120 Hz, which is the expected value. The 3dB bandwidth is about $\Delta\omega$ = 25 Hz, and the quality factor is 4.8. Such a low value quality factor indicates unpredicted damping which is currently under investigation.

3.2 Electrical measurement

The measured capacitance of the device is from 105 pF to about 655 pF. The results shows

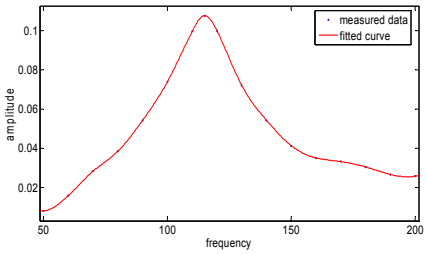

Fig.10 MMA measurement of the device with external mass

a parasitic capacitance of about 45 pF in the device. For V_T = 9 V and R_T = 10 MΩ, the output voltage was 230 mV, indicating a parasitic resistance of about 381 MΩ .

AC power measurement circuit is shown in Fig. 12. Two additional 10 pF capacitors C_T are used to block the DC path of the variable capacitor. Thus, the DC bias level of the output voltage is reduced to zero, eliminating the static power consumption of the device. A 9 V battery supply is used for V_T in this measurement.

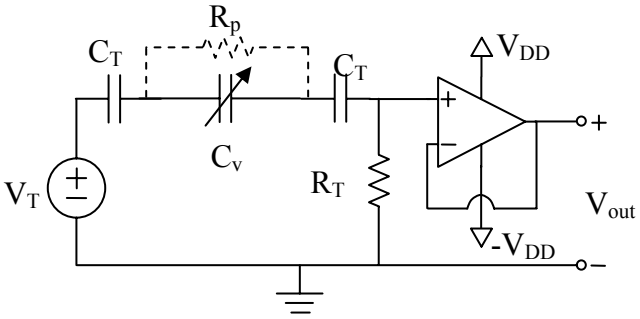

Fig. 12 Measured AC output power versus load resistance R_T

The measured output power versus R_T with no attached mass is plotted in Fig. 12. The vibration amplitude is maintained at about 6.25 m/s^2. The resonant frequency is 1730 Hz .The device has a relative displacement of about 18.2 µm, and C_{max} is estimated as 225 pF. The maximum output power is 0.42 µW when the load resistance R_T is about 5 MΩ. The power is lower than the

theoretical value due to the unstable vibration source.

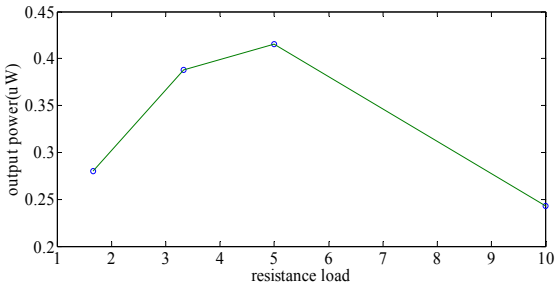

Fig. 12 Measured AC output power versus load resistance R_T

四、結論與討論

The design and analysis of a micro vibration-to-electricity energy converter with no external mass are accomplished. The modified device was successfully fabricated in the SOI wafer. By removing the overlap area and using LPCVD nitride, the parasitic resistance in the device was reduced. Timing can be controlled by adjusting parameter of the mechanical switch structure. Fabrication was successful and measurement is in progress.

This project was supported in part by the National Science Council, Taiwan, ROC, under the Grant No. NSC-96-2221-E-009-343.

五、參考文獻

[1] J.M. Rabaey, et al., “Picoradio supports ad hoc ultra low-power wireless networking”, IEEE Computer, Vol. 33, pp. 42-48, 2000.

[2] R. Tashiro, et al., “Development of an electrostatic generator that harnesses the motion of a living body: (use of a resonant phenomenon)”, JSME International Journal Series C, Vol. 43, No. 4, pp. 916-922, 2000.

[3] S. Roundy, et al., “Micro-electrostatic vibration-to-electricity converters,” Proc. IMECE 39309, 2002.

[4] R. Duggirala, et al., “Radioisotope micropower generator for CMOS self-powered sensor microsystems”, Proc. PowerMEMS 2004, pp. 133-136, 2004.

[5] T. Douseki, et al., “A batteryless wireless system uses ambient heat with a reversible-power-source compatible CMOS/SOI dc-dc converter”, Proc. IEEE International Solid-State Circuits Conference, pp. 2529-2533, 2003.

[6] Y. Chiu, et al., “MEMS design and fabrication of an electrostatic vibration-to-electricity energy converter,” Microsystem Technology, vol. 13, no. 11-12, pp. 1663-1669, 2007.

[7] Yi Chiu, et al., Microsystem Technology, vol. 13, no. 11-12, pp. 1663-1669, 2007.

[8] F. Peano, et al.,” Design and optimization of a MEMS electret-based capacitive energy scavenger,” Journal of Microelectromechanical Systems, vo.14,no.3, pp.429-435, 2005.

[9] P. Miteheson, et al.,” Architectures for vibration-driven micropower generators,” Journal of Microelectromechanical Systems, vo.13, no.3, pp.429-440, 2004.

[10] Yi Chiu, et al. “Capacitive vibration-to-electricity energy converter with integrated mechanical switches,” Power MEMS, pp.121-124, 2007